frontiers | Frontiers in Materials

TYPE Original Research
PUBLISHED 24 November 2022
DOI 10.3389/fmats.2022.995122

OPEN ACCESS

EDITED BY
Deepanraj B.,
Prince Mohammad bin Fahd University, Saudi Arabia

REVIEWED BY
Arkamitra Kar,
Birla Institute of Technology and Science, India
Tao Gu,
Southwest University of Science and Technology, China
Chengwen Wang,
China University of Petroleum, Huadong, China

*CORRESPONDENCE
Xiaowei Cheng,
chengxw@swpu.edu.cn

SPECIALTY SECTION
This article was submitted to Energy Materials, a section of the journal Frontiers in Materials

RECEIVED 15 July 2022
ACCEPTED 15 November 2022
PUBLISHED 24 November 2022

CITATION
Lian J, Wu Z, Lei Y, Gao Q, Mei K, Cai J and Cheng X (2022), Growth mechanism of carbonated tricalcium silicate (C_3S) under the high concentration of CO_2: A novel research for CCUS wells.
Front. Mater. 9:995122.
doi: 10.3389/fmats.2022.995122

Growth mechanism of carbonated tricalcium silicate (C_3S) under the high concentration of CO_2: A novel research for CCUS wells

Jihong Lian[1], Zhiqiang Wu[2], Yu Lei[3], Qiang Gao[4,5], Kaiyuan Mei[4,5], Jingxuan Cai[4,5] and Xiaowei Cheng[4,5]*

[1]CNOOC International Limited, Beijing, China, [2]CNOOC Research Institute Co. Ltd., Beijing, China, [3]China National Petroleum Corporation Southwest Oil and Gas Field Branch Exploration Division, Chengdu, China, [4]School of New Energy and Materials, Southwest Petroleum University, Chengdu, China, [5]State Key Laboratory of Oil & Gas Reservoir Geology and Exploitation, Southwest Petroleum University, Chengdu, China

Under the engineering background of the carbon dioxide capture and geological storage technology (CCUS) cementing project, an experiment on the generation of cement single-phase tricalcium silicate CO_2 carbonization products were carried out. Combining the phase diffraction pattern data and the thermogravimetric experiment, a relative crystallinity algorithm is proposed, which combines the quantitative results of the carbonized products with the relative crystallinity (RCP) results of each component. The growth and development mechanism of tricalcium silicate carbide crystal products under high temperature, high pressure and high concentration CO_2 environment is deduced. The experimental results show that under the conditions of early gas phase carbonization, the carbonization rate of C_3S first increases and then decreases as the carbonized crystal product grows. Under the conditions of early liquid phase carbonization, the carbonization rate of C_3S first decreases and then increases with the generation and fragmentation of the hydration barrier layer. It provides a research basis and a new perspective for the subsequent analysis of the changes in the microstructure of the cement paste in the carbonization process under the CCUS engineering background.

KEYWORDS

carbonization corrosion, relative crystallinity, single-phase cement, CCUS, C_3S (tricalcium silicate)

1 Introduction

The continuous consumption of fossil energy has led to a continuous increase in man-made CO_2 emissions. The International Energy Agency (IEA) predicts that by 2035, global CO_2 emissions will reach 35.4 billion tons (Chang et al., 2012). In the past 10 years, in order to effectively alleviate greenhouse gas emissions, carbon dioxide capture and

geological storage technology has become the main way to reduce CO_2 emissions and the greenhouse effect, and has received more and more attention (Bachu, 2008; Gleick et al., 2010; Leung et al., 2014). Portland cement is usually used in CCUS cementing projects (Kutchko et al., 2008; Duguid, 2009; Brandão et al., 2017). Cementing involves injecting cement slurry into the annulus between the casing and the formation, or between successive casings, and waiting for it to solidify to form cement paste to shield and seal the formation fluid. However, the cement-based materials in the well need to withstand the harsh service conditions of high temperature, high pressure, and high CO_2 concentration. Under such harsh conditions, cement-based materials will be in a process of accelerating carbonation. The formation of carbonized products and the growth and dissolution of crystals will cause changes in the pore structure of the cement matrix, and ultimately lead to cement performance failure (Groves et al., 1991; Dong et al., 2019). This will extremely seriously affect the integrity and safety of the long-term seal of the carbon dioxide storage technology. Therefore, it is necessary to conduct in-depth research on the carbonization mechanism of cement in the strongly acidic downhole environment to accurately predict the carbonization failure process of cement and provide a basis for the research and development of acid-resistant cement.

Portland cement mainly contains four single-phases: tricalcium silicate (C_3S), dicalcium silicate (C_2S), tricalcium aluminate (C_3A), and tetracalcium aluminoferrite (C_4AF) (Tadros et al., 1976; Sánchez Herrero et al., 2016; Cuesta et al., 2018). According to the American Petroleum Institute (API) standard, it can be known that C_3S is the main mineral component (50%–80%) in common oil well cement (G-class/H-class) (Sorrentino, 2008). In addition, the hydration and carbonization reaction of C_3S determines the development of the microstructure and structural strength of the cement paste (Groves et al., 1991; Mei et al., 2018). Therefore, to accurately predict the carbonization failure process of cement paste, it can be start with the single-phase tricalcium silicate, which has the greatest impact on the strength development of Portland cement (Kjellsen and Justnes, 2004). In the current research on the carbide carbonization process of tricalcium silicate, through conventional qualitative analysis (transmission electron microscope combined energy spectrometer (TEM-EDS), X-ray diffraction (XRD) and 29Si magic angle rotating nuclear magnetic resonance (^{29}Si MAS) -NMR). It has been proved that the product of fully carbonated C_3S is amorphous silicon dioxide (SiO_2) and calcite crystals and there will be no other polymorphic calcium carbonate ($CaCO_3$) (Li et al., 2018). In addition, a variety of technical methods (Rietveld refinement, thermogravimetric analysis, Fourier transform infrared spectroscopy, field emission scanning electron microscope and micro-Raman spectroscopy) have been used to study the growth process of calcite crystals produced after tricalcium silicate carbonization from the aspects of crystallite size, particle size, chemical bonds and thermodynamic stability (Wang et al., 2020; Klimavicius et al., 2021). Through these qualitative analyses, it can be known that the growth of calcite crystals formed by the carbonization of tricalcium silicate has a great influence on the strength of cement.

These existing studies focus on the qualitative analysis of the carbonization products of tricalcium silicate and the effect of the microstructure after complete carbonization on the changes in the macroscopic mechanical strength properties. However, the crystal growth of the carbonized product during the carbonization process of tricalcium silicate in a high-concentration CO_2 environment will seriously affect the development of its internal microstructure and macro-mechanical strength of cement. Due to insufficient research on the crystallization laws of single-phase cement crystal products after CO_2 carbonization, there is insufficient understanding of the changes in the microstructure of cement after CO_2 carbonization. There are few studies on the orientation of the cement crystal phase after CO_2 carbonization, or the crystallization and crystal transformation laws in the long-term carbonization process, and there is no quantitative or semi-quantitative method to describe the growth process of carbonized crystalline products. In this paper, according to the crystal change law of single-phase cement during CO_2 carbonization, the C_3S hydration products and carbonization products were analyzed by X-ray diffraction (XRD) analysis, and the relative crystallinity was introduced according to the experimental results for semi-quantitative analysis. The changes of amorphous products during the hydration and carbonization of C_3S were investigated by thermogravimetric (TG/DTG) analysis, and the relative crystallinity change law of C_3S single-phase cement CO_2 carbonization crystal products was studied. It is expected to provide new ideas and research basis for the study of microstructure changes caused by crystal changes.

2 Materials and methods

2.1 Materials

C_3S single-phase cement powder was provided by Mineral Research Processing (M.R. PRO, France).

2.2 Experiment methods

The water-cement ratio provided by the API standard is 0.38–0.44. The effect of the water-cement ratio on cement particle hydration was mainly reflected in the cement particle spacing and in the final degree of hydration reaction, owing to the rapid hydration of the single phase, in order to ensure that the sample has a certain fluidity for moulding, a water-cement ratio of 0.6 was selected to prepare single-phase cement samples with different carbonization time intervals at 90°C (Mei et al., 2018).

FIGURE 1
Photograph and schematic representation of HTHP carbonation kettle and sample loading.

TABLE 1 Experimental conditions of the sample.

Corrosive environment	Experiment temperature (°C)	The reaction time (days)	Samples
Gas phase	90	1, 3, 7, 14, 28	GA-1, GA-3, GA-7, GA-14, GA-28
Liquid phase			LA-1, LA-3, LA-7, LA-14, LA-28

In general oil and gas well conditions, the corrosive medium CO_2 usually exists in two states: one is in the form of a solute dissolved in formation water, and the other is in the form of supercritical gaseous CO_2 in a humid environment. To study the influence of these two different water-humidity environments on the carbonation process of the samples, the prepared samples were placed in a high-temperature and high-pressure carbonation reactor, as shown in Figure 1. The upper sample is in a gas-phase environment as a dry gas carbonization environment, and the lower sample is in a liquid phase environment as an acid solution environment. CO_2 gas with high pressure of 5.0 MPa (3.0 MPa for air and 8.0 MPa for total pressure) was injected to ensure saturation conditions, thereby simulating the underground environment (Mei et al., 2021).

During the experiment, load the prepared single-phase cement slurry into the kettle body, the assembled kettle body was immersed in a constant-temperature water-bath curing box to maintain the experimental temperature of the sample. The single-ore cement carbonization curing environment, temperature, and age are listed in Table 1. The selection of experimental temperature conditions is based on the formation depth-temperature relationship to simulate the temperature conditions under common well depth environments.

2.3 Characterization

To evaluate the carbonization products of the CO_2 carbonized samples in the early stage of the experiment and the microstructure changes after carbonization, the reaction of the samples was stopped by soaking them in isopropanol. The immersion time of the carbonized sample was defined as from the completion of the carbonization corrosion experiment to immediately before the inspection, and the following tests were carried out:

1) Grind all CO_2 carbonized samples (hand-grind with a grinder), and then use an X-ray diffractometer for phase analysis. The equipment model is DXJ-2000, and the place of production is China's Fangyuan Instrument Co., Ltd. When the equipment is performing phase analysis, the current is 20 mA and the voltage is 30 kV. The sample passes in 2θ at a rate of 0.04°/s in the range of 5°–70°.
2) A Thermogravimetric analysis (DTG) (TGA/SDTA851e, Mettler Toledo, Switzerland, TA Q20) was carried out to quantitatively investigate the carbonation products over a temperature range of 40°C–1,000°C at a heating rate of 10°C/min. Additionally, the powder samples were tested using nitrogen gas as the working gas.

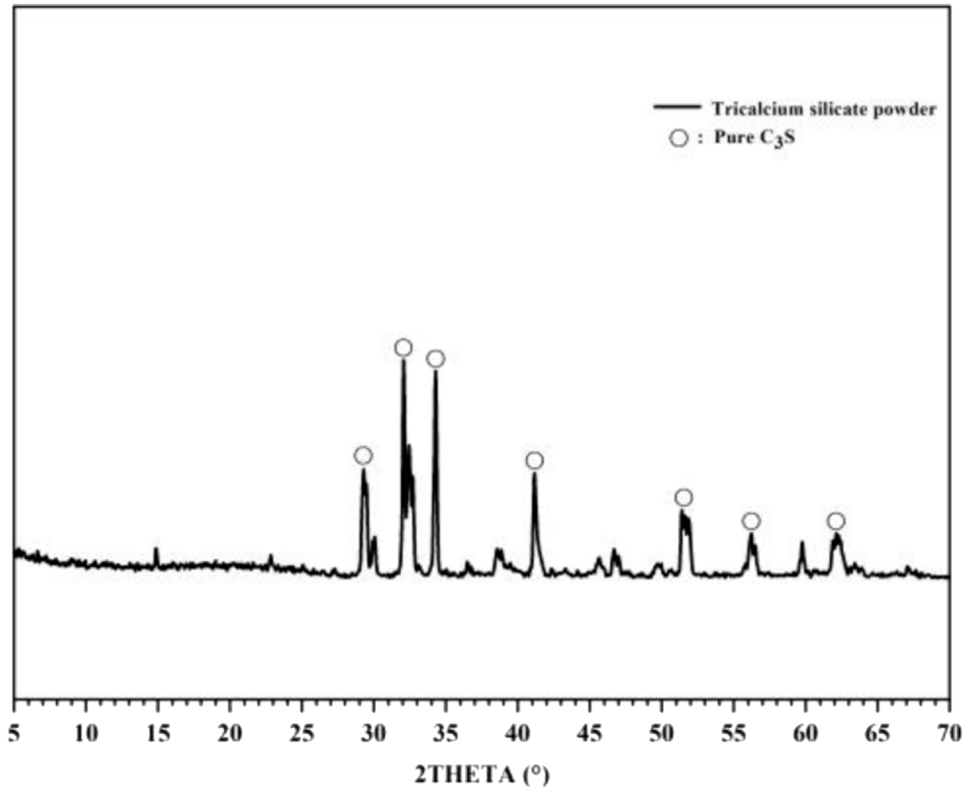

FIGURE 2
XRD results of experimental powders and main crystal faces.

3 Results and discussion

3.1 Material property

The X-ray diffraction (XRD) peaks of these experiments with the standard powder diffraction pattern (PDF# 49-0442) are consistent with Figure 2. The particle size distribution of the powder was measured using a laser particle size analyser (Mastersizer 2000; Malvern Panalytical, United Kingdom), and its main physical properties are shown in Figure 3. The particle size was mainly concentrated in the range of 1–100 μm, the specific surface area was 1.09 m^2/g, and the median size was 6.365 μm.

3.2 Phase analysis

For the XRD diffractograms shown in Figure 4, carbonation C_3S samples (GA-1, 3, 7, 14, 28 and LA-1, 3, 7, 14, 28) with different curing times under liquid and gas phase carbonization conditions (CH: #44-1,481 and Calcite: #47-1743). It can be seen from the figure that calcite $CaCO_3$ (abbreviated as C $\bar{C}$) is the main carbonization product of tricalcium silicate, and the hydrated product of tricalcium silicate, calcium hydroxide (abbreviated as CH), gradually decreases and disappears with the extension of the carbonization curing time.

The amorphous gel phase calcium silicate hydrate (abbreviated as C-S-H) is one of the products of cement hydration process, but the XRD test cannot effectively characterize the amorphous gel phase. Therefore, it is necessary to combine the decomposition temperature of the phase at different temperatures to characterize the phase, where 400°C–500°C is the decomposition interval of the hydration product CH, and 600°C–900°C is the decomposition interval of the CO_2 carbonization product (Gomez-Villalba et al., 2012). The decomposition temperature range and decomposition stage of single-phase C_3S cement hydration and carbonization products are shown in Table 2.

The quality loss in the range of 120°C and 460°C are produced by the decomposition of C-S-H and CH, respectively. At the same time, the CH produced by C_3S hydration is consumed in large quantities due to the carbonization reaction, and a large amount of $CaCO_3$ is produced. The quality loss in the range of 750°C is produced by C $\bar{C}$ decomposition (Wei et al., 2022). Through synergistic analysis with the thermogravimetric Figure 5 TG characterisation results, compared with the XRD calibration sample, it can be seen that the carbonization products of C_3S are all calcite calcium carbonate.

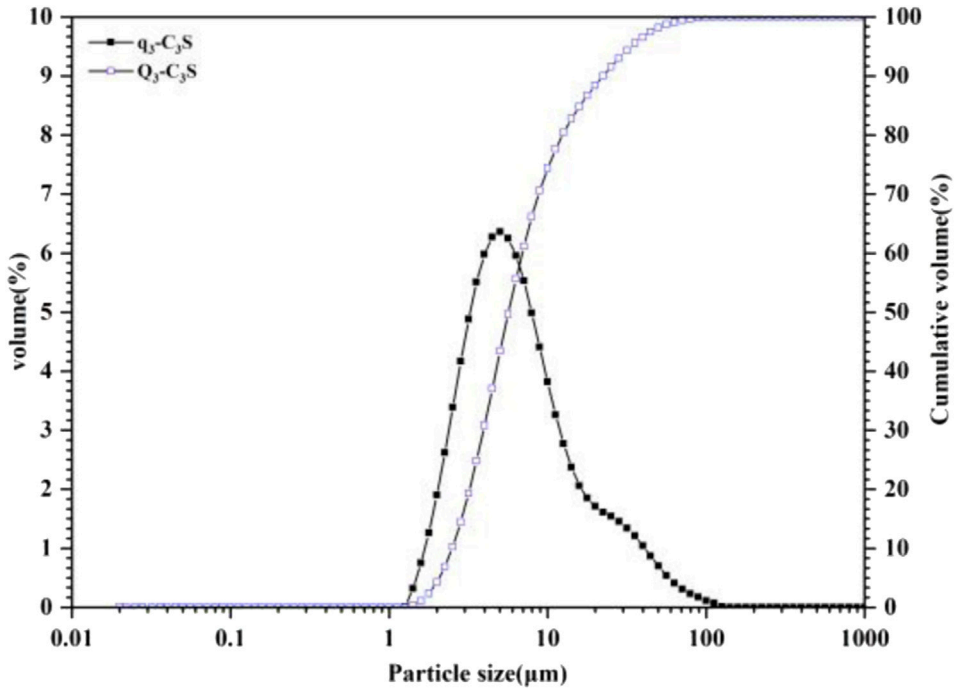

FIGURE 3
Particle size distribution of C_3S single-phase raw materials.

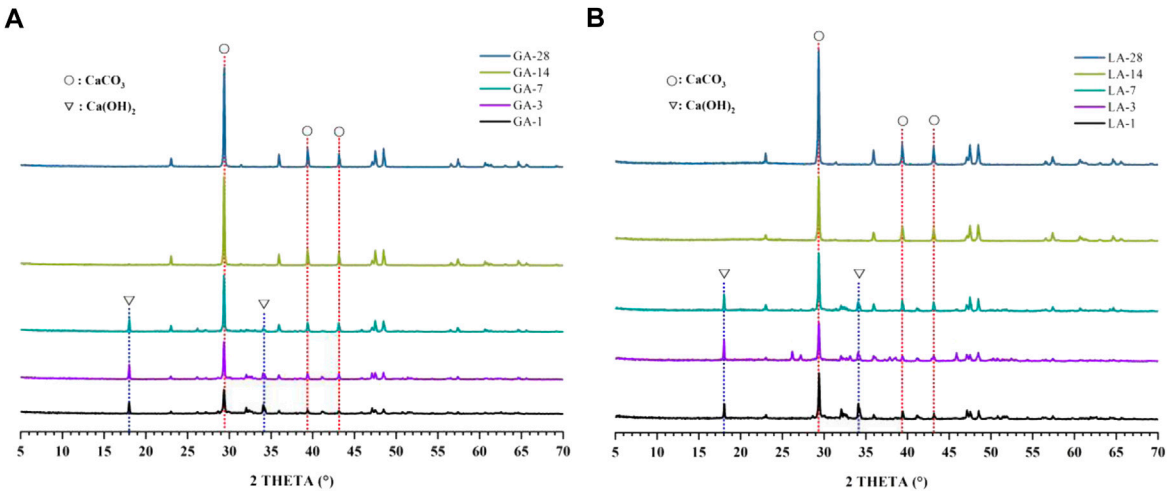

FIGURE 4
(A). XRD pattern of the GA-1, 3, 7, 14, 28 samples; **(B)**. XRD pattern of the LA-1, 3, 7, 14, 28 samples.

3.3 Relative crystallinity analysis

The main product after full hydration reaction of tricalcium silicate is composed of gel phase C-S-H and CH phase with different crystallinity (Cuesta et al., 2018). These hydration products are carbonized under the conditions of high concentration of carbon dioxide. The carbonized crystal products produced by the carbonization reaction will have a

TABLE 2 Decomposition temperature range and decomposition phases in C_3S carbonization samples of single-phase cement.

Constituent	Abbreviation	Decomposition temperature (°C)	Decomposition products
$Ca_5Si_6O_{16}(OH)\cdot 4H_2O$	C-S-H	110–180	H_2O
$Ca(OH)_2$	CH	400–500	H_2O
$CaCO_3$	C $\bar{C}$	600–900	CO_2

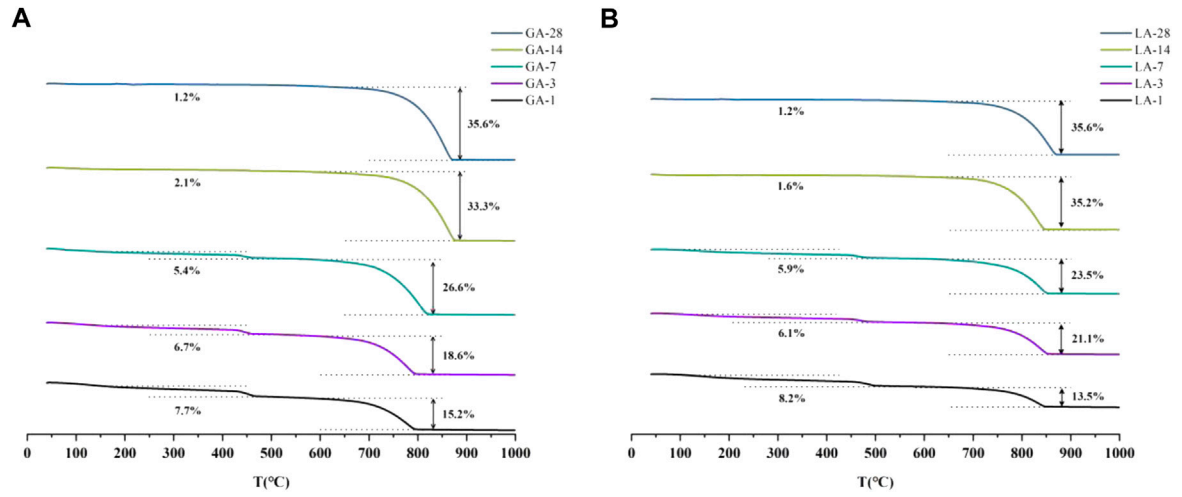

FIGURE 5
(A) TG diagram of GA-1, 3, 7, 14, 28 samples; **(B)** TG diagram of LA-1, 3, 7, 14, 28 samples.

significant impact on the structure of the tricalcium silicate single-phase cement slurry. Therefore, studying the dependence of crystalline hydration products on carbonized crystalline products can enable people to understand the properties of cement paste structure carbonization corrosion damage. After long-term carbonization, the hydration products of cement continue to decrease, and the carbonization products continue to increase. In order to explore the changes in the crystallization law of the product crystals during the CO_2 carbonization process, the relative crystallinity can be introduced to conduct a semi-quantitative analysis of the development process of the carbonized crystallization products, so as to compare the crystal phases in the C_3S carbonization reaction products of cement single phase and determine the law.

By measuring the cumulative diffraction intensity of the crystalline phases, a semi-quantitative analysis of the crystallinity changes of the phases was carried out, and the law of changes in the crystal structure was obtained (Dai et al., 2017; Dai et al., 2018). The crystallization process of tricalcium silicate carbonized products is related to the carbonization environment temperature and carbonization age. With regard to the phase growth process of the crystalline product, there is no perfect crystal owing to the influence of the external environment. Therefore, the crystallinity mentioned in this article is all relative crystallinity (Capron et al., 1987; Kontoyannis and Vagenas, 2000; Lee et al., 2008; Jiang et al., 2018), where the relative crystallinity is related to the crystallinity of the reference phase taken. The crystallinity of the phase is represented by the main diffraction peak area, I, corresponding to the object in the diffraction test result. The relative crystallinity of a single crystalline phase relative to all crystalline phases in the sample (RCS) and relative crystallinity of the phase (RCP) of a single carbonized crystalline phase under certain curing conditions were used to understand the crystal change process of carbonization products in a single cement phase. The calculation process of the RCS and RCP of the crystalline phase is shown in Eqs 1–4.

$$I_{SUM-phase} = \sum_{n=1}^{3} I_{n-phase} \quad (1)$$

$$I_{SUM} = \sum I_{SUM-phases} \quad (2)$$

$$RCS = \frac{I_{SUM-phase}}{I_{SUM}} \times 100\% \quad (3)$$

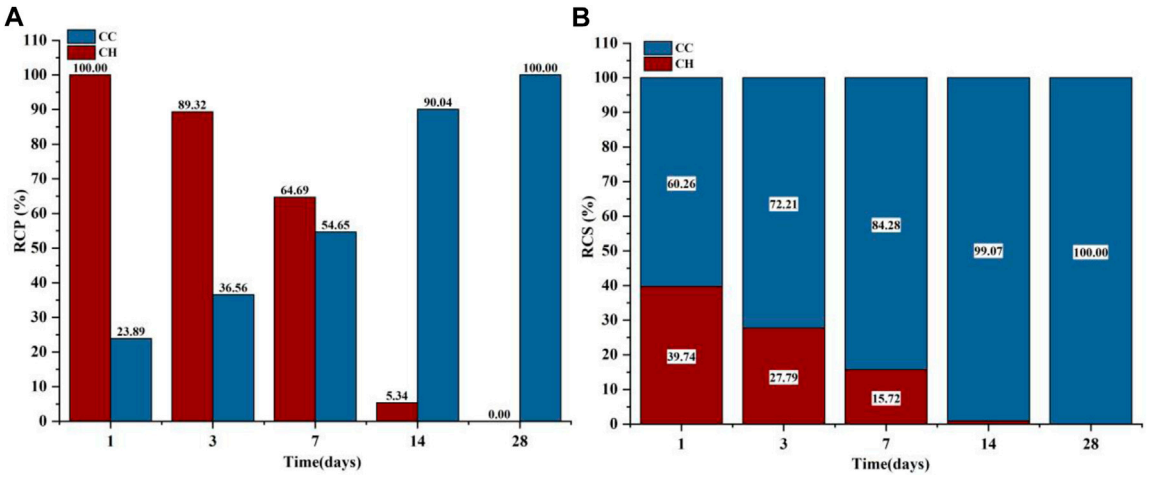

FIGURE 6
GA-1,3,7,14,28 Samples: **(A)** Carbonized crystalline product RCP; **(B)** Carbonized crystalline product RCS.

$$RCP = \frac{I_{SUM-phase}}{\max\limits_{t} I_{SUM-phase}} \times 100\% \quad (4)$$

$I_{n\text{-}phase}$ is the peak area of the n-phase diffraction peak corresponding to a certain phase; $I_{SUM\text{-}phase}$ is the sum of the integrated areas of the three strongest peaks in the diffraction peak of a certain phase, and I_{SUM} is the sum of the integrated area of the diffraction peaks of the crystal phase in a certain sample. RCP = 100% indicates the maximum integral area of the diffraction peak of hydration or carbonization products during the carbonization age. This suggests that the crystal structure of the crystalline phase in the sample is relatively complete. Jade software (version 6.0) was used to subtract the background peaks of the amorphous phase in the test results, fit each peak of the main crystalline product to obtain the three characteristic peaks with the strongest phase intensity, and calculate the integral area. The RCS and RCP values of the crystalline phase were calculated using Eqs 1–4, and the specific sample analysis results are as follows.

3.3.1 Analysis of relative crystallinity change under gas phase carbonization

The phases of C_3S after gas-phase carbonization at 90°C are shown in Figure 4A. The main hydration and carbonization phases were CH and C $\overline{C}$; and the intensity of the diffraction peaks changed continuously with the increase in carbonization age. For CH, which is the phase consumed in the carbonization process, its diffraction peaks disappeared after 14 days; the increasing peak of C $\bar{C}$ indicates that the amount of crystals and relative crystallinity also increased. The specific results are shown in Figure 6. The RCP of CH was highest after 1 day of reacting, then continuously decreased to only 5.34% at 14 days, disappearing at 28 days. The RCP for the corresponding carbonization product C $\bar{C}$ increased continuously from 23.89% at 1 day, reaching a maximum at 28 days. The RCS changes in C_3S were consistent with the RCP results. The RCS ratio of C $\bar{C}$ continuously increased, reaching its highest value at 28 days, and the RCS of CH was almost reduced to zero at 14 days and was completely consumed. Clearly, the crystals formed by the hydration product CH continued to decrease in the sample, indicating that although the carbonization reaction did not completely consume the hydration product, the carbonization product formed crystals. The crystalline phase change in C_3S is mainly due to the change from CH to C $\bar{C}$. Since the main carbonization product C $\bar{C}$ is a high-strength phase, it also has greater brittleness (Marius-George et al., 2021; Poudyal et al., 2021). The formation of brittle phase will adversely affect the mechanical properties of cement.

Because both the CO_2 carbonization and hydration processes react with Ca^{2+} to produce the corresponding products, the sum of the C $\overline{C}$ and CH products represents the degree of C_3S hydration and C_3S carbonization reaction. CO_2 carbonization product quantitative test DTG curve and content of each component of vapour phase carbonization samples are shown in Figure 7 (thermogravimetric analysis). As the carbonization age increased, the quantity of carbonization products continued to increase, to 59.19% at 28 days. The hydration products had been decreasing since the start of carbonization, and 4.03% remained at 28 days; at the same time, according to the image, under this carbonization condition, the carbonization rate was high at first and then decreased. In addition, when the carbonization age was 1 day, the sample already contained 33.93% carbonization products, indicating that the hydration process was affected by CO_2 carbonization. The quantitative

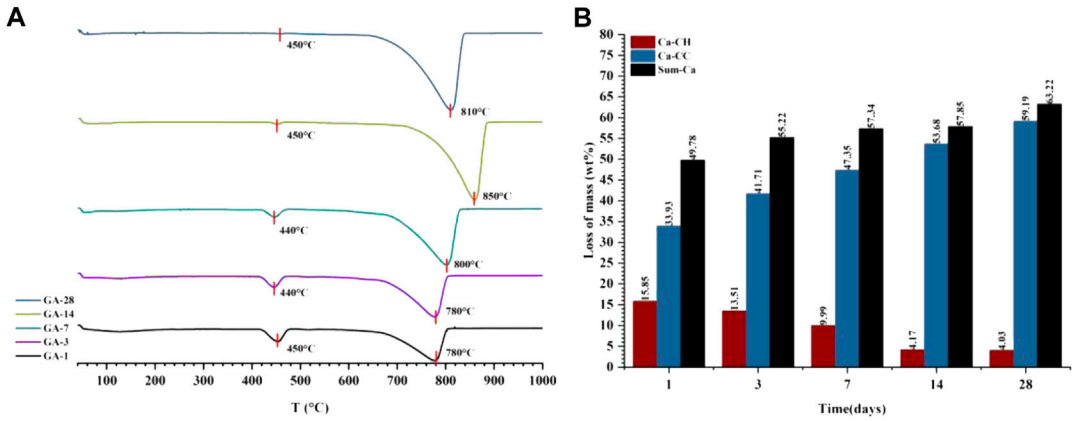

FIGURE 7
The DTG curve **(A)** and the content of each component in the quantitative tests of CO_2 carbonization products **(B)** of the gas phase carbonization sample (GA-1, 3, 7, 14, 28).

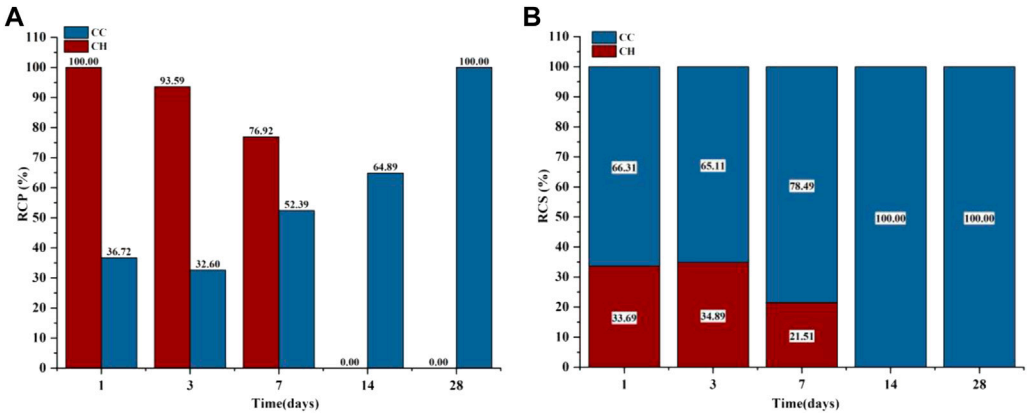

FIGURE 8
LA-1, 3, 7, 14, 28 samples: **(A)** Carbonized crystalline product RCP; **(B)** Carbonized crystalline product RCS.

analysis results of the carbonization products are consistent with the above RCS analysis results.

3.3.2 Analysis of relative crystallinity change under liquid phase carbonization

Figure 4B shows the XRD test results of the liquid-phase carbonized sample and the RCP and RCS results of the crystalline product. The phases contained in the C_3S liquid-phase carbonization sample at 90°C are mainly CH and C $\bar{C}$. It can also be seen from Figure 4B that the diffraction peak of CH disappeared in 14 days, which indicates that the CH crystals in the sample at this time were lower than the minimum XRD detection amount. The intensity of the diffraction peak corresponding to the carbonization product C $\bar{C}$ increased with the carbonization age. From the change rule of RCP in Figure 8A, the RCP of CH continued to decrease from 1 to 7 days, and 76.92% remained at 7 days, but CH disappeared at 14 days. The corresponding product C $\bar{C}$ changed little at 1–3 days, then continued to increase, and the RCP reached a maximum at 28 days. As shown in Figure 8B, the RCS of the CH and C $\bar{C}$ crystals in the sample remained unchanged after 1–3 days. Subsequently, CH was greatly consumed by the corrosive medium CO_2. At 7 days, the RCS of CH in the sample was only 21.51%, and the experiment after 14 days of carbonization did not contain the crystalline CH phase. The TG results also show that the amount of CH in the samples with a

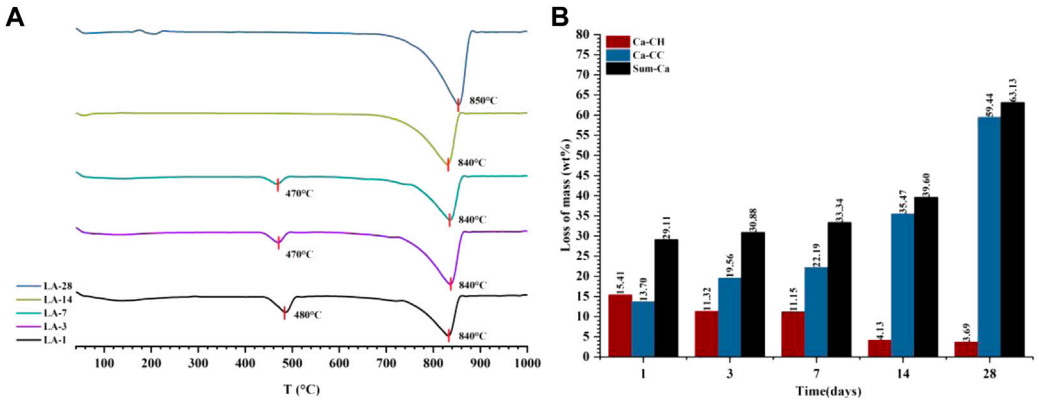

FIGURE 9
The DTG curve **(A)** and the content of each component in the quantitative test of CO_2 carbonization products **(B)** of the liquid phase carbonization sample (LA-1, 3, 7, 14, 28).

carbonization age of 14 days is already very small and can be ignored.

Combining the results of thermogravimetric analysis to verify the carbonization law shown by the relative crystallinity is shown in Figure 9. The hydration product CH was at a maximum of 15.41% at 1 day, and then continued to decrease to only 3.69% at 28 days, so the decomposition peak of CH on the DTG curve disappeared. For C $\overline{C}$, the increase was slower at 1–7 days, from 13.70% to 35.47%, and it increased rapidly at 14–28 days, which was much greater than the consumption of CH, and its content was 59.44% at 28 days. From Sum-Ca (Calcium-containing phases participating in the reaction), 39.60% at 14 days is far less than 63.13% at 28 days, so the C_3S reaction at 14 days was not complete. This shows that because of carbonization, the hydration process of C_3S is greatly affected, and the consumption rate of hydration products is slower than the rate of the carbonization reaction. The quantitative analysis results of the carbonization products are consistent with the above RCS analysis results of liquid carbonization.

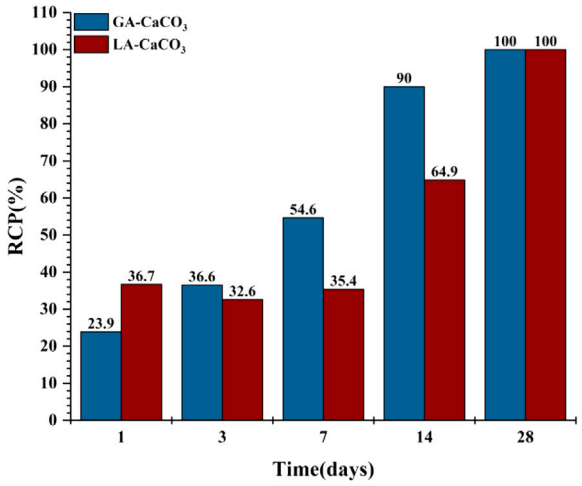

FIGURE 10
RCP variation law of the carbonization crystallization product C $\overline{C}$ of GA-LA sample.

3.4 Analysis of carbonization product crystal change process

The foregoing is the law of influence on the crystal products formed in the CO_2 carbonization reaction of C_3S mono-ore cement under different corrosive environments, including CH generated by the hydration reaction. Among the carbonization products, C $\overline{C}$ was the main crystalline phase. Crystallisation and crystal changes have a greater impact on the internal structure. On the one hand, because the RCS of the crystalline phase is based on the relative crystallisation between the phases in the sample, the explanation of the change in the crystalline phase with time is weak; on the other hand, the RCP of the crystalline phase is based on the carbonization age. The phase with the highest crystallinity was used as a reference, and the relative crystallinity of the crystal phase changed with time. Therefore, the RCP of the main carbonization product, C $\overline{C}$, is used to discuss its crystallisation law.

The main crystalline phase of C_3S formed by CO_2 carbonization is C $\overline{C}$, and no other crystal-type carbonization products are formed. As shown in Figure 10 in a gas-phase CO_2 carbonization environment, the initial RCP value of C $\overline{C}$ is low at 1–3 days. At 7–14 days, the carbonization product crystallisation speed increases, and then during carbonization at 14–28 days the

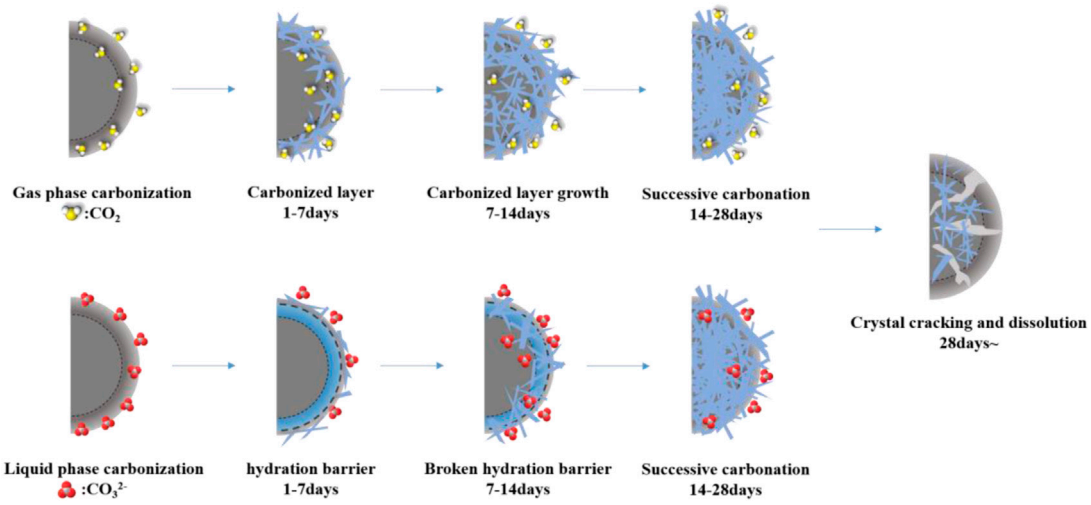

FIGURE 11
Schematic diagram of CO_2 carbonization process of C_3S single-phase cement.

crystallisation rate of the product slows down. Combined with previous studies (Niel and Eurybiades, 1982; Palmer et al., 1988; Zuddas et al., 2003; Therese et al., 2011; Der, 2014), This is because in the early stage of gas phase carbonization, there is a mass space between the C_3S particles and no binding phase is formed, and the moist CO_2 gas can penetrate into the sample unimpededly and the gas permeation rate is fast. In the later stage of gas-phase carbonization, with the formation of carbonized crystalline products, the void ratio of the C3S single ore sample decreases, which reduces the chance of contact between C_3S and CO_2.

In the liquid phase CO_2 carbonization environment, the RCP value of the carbonization products decreased from 1 to 3 days, then the liquid phase carbonization reaction speed continued to increase. Combined with the quantitative results, the hydration products at this stage increased, indicating that delayed hydration destroys the integrity of the carbonization product crystals, resulting in a decrease in the RCP. According to previous studies (Goodbrake et al., 1979), this is due to the faster hydration of C_3S in the liquid phase environment, and more CH phase and C-S-H are formed at the beginning of the carbonization reaction. In the subsequent reaction, the presence of a large amount of free Ca^{2+} during the hydration process is conducive to the reaction with CO_3^{2-}. It can still form a stable carbonization product even in an environment with a higher concentration of CO_2, and there are only C $\overline{C}$ crystals in C_3S. After the carbonization product crystals nucleate, they continue to grow as the carbonization medium continues to diffuse and react. When CH is carbonated, the volume will increase by about 11.23% (Mei et al., 2018), which will severely expand the cracks along with the carbonation reaction. The crack will continue to expand until the crystal breaks. This led to the acceleration of the later liquid phase carbonization.

For C-S-H, although the gel phase does not have a fixed molecular formula, many studies (Rostami et al., 2012; Morandeau et al., 2014; Shen et al., 2016) have shown that as C-S-H is corroded by CO_2, when the amount of C-S-H is small, the volume of C-S-H will increase, and the volume effect of C-S-H accounts for 70% of the total volume change. When the amount of C-S-H is large, the volume of C-S-H decreases after carbonization, resulting in sample shrinkage. Combined with the previous quantitative analysis of the reaction products, the amount of C-S-H is relatively low; when it is corroded by CO_2, it is mainly due to volume expansion, and a hydration barrier layer (the reduction of porosity and the dense growth of CHS under the early liquid phase environment carbonization) is formed on the surface of the cement paste to slow down the carbonization process. Numerous studies (Fabbri et al., 2012; Cheshire et al., 2017; Jimoh et al., 2018; Shah et al., 2018) have shown that the change in pore structure affects the penetration process of the CO_2 corrosive medium to a certain extent, thus delaying the carbonization process. Therefore, the RCP value of vapour-phase carbonization at 14 days is much larger than that of liquid-phase carbonization. In summary, the entire CO_2 cement single-ore carbonization process (Mei et al., 2018) is shown in the model in Figure 11.

4 Conclusion

In this study, XRD and relative crystallinity algorithms were used to analyse and study the relative crystallinity change law of C_3S single-phase cement during CO_2 carbonization. The main conclusions are as follows.

1) Compared with gas phase carbonization, the formation rate of liquid phase carbonization crystallization products is slower. The increase of carbonization time will accelerate the formation of crystallization products. For subsequent cement failure, the liquid phase environment is more dangerous.
2) Under the assumption that all carbonization products are crystals, the quantitative results of the carbonization products and the relative crystallinity (RCS) results of the components are combined to deduce the crystal change process of the carbonization products during the CO_2 carbonization process. Supported by previous research results, this semi-analytical method is feasible and more intuitive. In the CCUS well condition, the carbonization products of cement will dissolve in the later stage, and the development trend of the later carbonization products can be predicted by the calculation results of the relative crystallinity.
3) The method of calculating relative crystallinity combined with thermogravimetric analysis can realize semi-quantitative analysis of the pre-development process of carbonized product crystals in the process of tricalcium silicate carbonization. The effect of this analysis method is intuitive, it provides a good analysis method to explore the evolution process of the crystal growth of carbonized corrosion products.

The above results provide a research basis for analysing the microstructural changes in cement paste caused by CO_2 carbonization and provides a new analysis perspective of XRD combined with relative crystallinity algorithm for carbonization research.

Data availability statement

The raw data supporting the conclusion of this article will be made available by the authors, without undue reservation.

Author contributions

JL: Conceptualization, investigation, writing-original draft, data curation ZW: Validation, resources, writing—review & editing, supervision. YL: Validation, formal analysis, investigation, data curation QG: Formal analysis, project administration KM: Formal analysis, project administration XC: Resources, funding acquisition JC: Methodology, conceptualization.

Funding

This study was financially supported by 111 Project, No. D18016. The Sichuan Science and Technology Program (2021YFQ0045 and 2021YFSY0056) and the Cnooc's preliminary project: Feasibility study of Wenchang 9-7 oilfield (2021PFS-05).

Acknowledgments

The authors appreciate the support of the Sichuan Science and Technology Program (2021YFQ0045 and 2021YFSY0056) and the Cnooc's preliminary project: Feasibility study of Wenchang 9-7 oilfield (2021PFS-05). The authors would also like to thank the Advanced Cementing Materials Research Center of SWPU for their kind assistance with the experiments.

Conflict of interest

JL was empolyed by the CNOOC International Limited, ZW was empolyed by CNOOC Research Institute Co. Ltd., and YL was empolyed by the China National Petroleum Corporation Southwest Oil and Gas Field Branch Exploration Division.

The remaining authors declare that the research was conducted in the absence of any commercial or financial relationships that could be construed as a potential conflict of interest.

Publisher's note

References

Bachu, S. (2008). CO2 storage in geological media: Role, means, status and barriers to deployment. *Prog. Energy Combust. Sci.* 34 (2), 254–273. No. doi:10.1016/j.pecs.2007.10.001

Brandão, N. B. A., Roehl, D. A. B., de Andrade Silva, F. B., and Rosas E Silva, R. B. (2017). The impact of cement slurry aging creep on the construction process of oil wells. *J. Pet. Sci. Eng.* 157, 422–429. doi:10.1016/j.petrol.2017.07.051

Capron, B., Girou, A., Humbert, L., and Puech-Costes, E. (1987). Experimental dissolution of natural calcite. II. A matrix optimized for study of the relative influence of carbon dioxide pressure, salinity, lithostatic pressure, granulometry, crystallinity, and flow rate. *Bull. Soc. Chim. Fr.*

Chang, Y., Lee, J., and Yoon, H. (2012). Alternative projection of the world energy consumption-in comparison with the 2010 international energy outlook. *Energy Policy* 50, 154–160. doi:10.1016/j.enpol.2012.07.059

Cheshire, M. C., Stack, A. G., Carey, J. W., Anovitz, L. M., Prisk, T. R., and Ilavsky, J. (2017). Wellbore cement porosity evolution in response to mineral alteration during CO2 flooding. *Environ. Sci. Technol.* 51 (1), 692–698. No. doi:10.1021/acs.est.6b03290

Cuesta, A., Zea-Garcia, J. D., Londono-Zuluaga, D., De la Torre, A. G., Santacruz, I., Vallcorba, O., et al. (2018). Multiscale understanding of tricalcium silicate hydration reactions. *Sci. Rep.* 8 (1), 8544. doi:10.1038/s41598-018-26943-y

Dai, Y., Zou, H., Zhu, H., Zhou, X., Song, Y., Shi, Z. S., et al. (2017). Controlled synthesis of calcite/vaterite/aragonite and their applications as red phosphors doped with Eu^{3+} ions. *CRYSTENGCOMM* 19 (20), 2758–2767. No. doi:10.1039/c7ce00375g

Dai, Y., Zou, H., Zhu, H., Zhou, X., Song, Y., Zheng, K., et al. (2018). Facile surfactant- and template-free synthesis and luminescence properties of needle-like calcite CaCO3:Eu3+ phosphors. *CRYSTENGCOMM* 20 (4), 496–504. No. doi:10.1039/c7ce01554b

Der, W. (2014). Calcite growth: Rate dependence on saturation, on ratios of dissolved calcium and (bi)carbonate and on their complexes(Article). *J. Cryst. GROWTH* 394, 137–144.

Dong, S., Berelson, W. M., Rollins, N. E., Subhas, A. V., Naviaux, J. D., Celestian, A. J., et al. (2019). Aragonite dissolution kinetics and calcite/aragonite ratios in sinking and suspended particles in the North Pacific. *Earth Planet. Sci. Lett.* 515, 1–12. doi:10.1016/j.epsl.2019.03.016

Duguid, A. (2009). An estimate of the time to degrade the cement sheath in a well exposed to carbonated brine. *Energy Procedia* 1 (1), 3181–3188. No. doi:10.1016/j.egypro.2009.02.101

Fabbri, A., Jacquemet, N., and Seyedi, D. M. (2012). A chemo-poromechanical model of oilwell cement carbonation under CO_2 geological storage conditions(Article). *Cem. Concr. Res.* 42 (1), 8–19. No. doi:10.1016/j.cemconres.2011.07.002

Gleick, P. H., Adams, R. M., Amasino, R. M., AndErs, E., Anderson, D. J., Anderson, W. W., et al. (2010). Climate change and the integrity of science. *SCIENCE* 2010 (5980), 689–690. No doi:10.1126/science.328.5979.689

Gomez-Villalba, L. S., Lopez-Arce, P., Alvarez De Buergo, M., and Fort, R. (2012). Atomic defects and their relationship to aragonite–calcite transformation in portlandite nanocrystal carbonation. *Cryst. Growth Des.* 12 (10), 4844–4852. No. doi:10.1021/cg300628m

Goodbrake, C. J., Young, J. F., and Berger, R. L. (1979). Reaction of hydraulic calcium silicates with carbon dioxide and water. *J. Am. Ceram. Soc.* 62 (9-10), 488–491. No.. doi:10.1111/j.1151-2916.1979.tb19112.x

Groves, G. W., Brough, A., Richardson, I. G., and Dobson, C. M. (1991). Progressive changes in the structure of hardened C_3S cement pastes due to carbonation. *J. Am. Ceram. Soc.* 74 (11), 2891–2896. No. doi:10.1111/j.1151-2916.1991.tb06859.x

Jiang, J., Zheng, Q., Hou, D., Yan, Y., Chen, H., She, W., et al. (2018). Calcite crystallization in the cement system: Morphological diversity, growth mechanism and shape evolution. *Phys. Chem. Chem. Phys.* 20 (20), 14174–14181. No. doi:10.1039/c8cp01979g

Jimoh, O. A., Ariffin, K. S., Hussin, H. B., and Temitope, A. E. (2018). Synthesis of precipitated calcium carbonate: A review. *Carbonates Evaporites* 33 (2), 331–346. No. doi:10.1007/s13146-017-0341-x

Kjellsen, K. O., and Justnes, H. (2004). Revisiting the microstructure of hydrated tricalcium silicate––a comparison to Portland cement. *Cem. Concr. Compos.* 26 (8), 947–956. No. doi:10.1016/j.cemconcomp.2004.02.030

Klimavicius, V., Hilbig, H., Gutmann, T., and Buntkowsky, G. (2021). Direct observation of carbonate formation in partly hydrated tricalcium silicate by dynamic nuclear polarization enhanced NMR spectroscopy. *J. Phys. Chem. C* 125 (13), 7321–7328. No. doi:10.1021/acs.jpcc.0c10382

Kontoyannis, C. G., and Vagenas, N. V. (2000). Calcium carbonate phase analysis using XRD and FT-Raman spectroscopy. *Analyst* 125 (2), 251–255. No. doi:10.1039/a908609i

Kutchko, B. G., Strazisar, B. R., Dzombak, D. A., Lowry, G. V., and Thaulow, N. (2008). Degradation of well cement by CO2 under geologic sequestration conditions. *Environ. Sci. Technol.* 41 (13), 4787–4792. No. doi:10.1021/es062828c

Lee, M., Hodson, M., and Langworthy, G. (2008). Crystallization of calcite from amorphous calcium carbonate: Earthworms show the way. *Mineral. Mag.* 72 (1), 257–261. No. doi:10.1180/minmag.2008.072.1.257

Leung, D., Caramanna, G., and Maroto-Valer, M. (2014). An overview of current status of carbon dioxide capture and storage technologies. *Renew. Sustain. Energy Rev.* 39, 426–443. doi:10.1016/j.rser.2014.07.093

Li, Z., He, Z., and Shao, Y. (2018). Early age carbonation heat and products of tricalcium silicate paste subject to carbon dioxide curing. *MATERIALS* 11 (5), 730. doi:10.3390/ma11050730

Marius-George, P., Georgeta, V., Alina-Ioana, B., Eugeniu, V., and Vasile, E. (2021). CO_2 sequestration in the production of portland cement mortars with calcium carbonate additions. *Nanomater. (Basel, Switz.* 11 (4), 875. No. doi:10.3390/nano11040875

Mei, K., Cheng, X., Gu, T., Zheng, Y., Gong, P., Li, B., et al. (2021). Effects of Fe and Al ions during hydrogen sulphide (H_2S)-induced corrosion of tetracalcium aluminoferrite (C_4AF) and tricalcium aluminate (C_3A). *J. Hazard. Mat.* 403, 123928. doi:10.1016/j.jhazmat.2020.123928

Mei, K., Cheng, X., Zhang, H., Yu, Y., Gao, X., Zhao, F., et al. (2018). The coupled reaction and crystal growth mechanism of tricalcium silicate (C3S): An experimental study for carbon dioxide geo-sequestration wells. *Constr. Build. Mat.* 187, 1286–1294. doi:10.1016/j.conbuildmat.2018.08.080

Morandeau, A. A., Morandeau, I., Thiéry, M., and Dangla, P. (2014). Investigation of the carbonation mechanism of CH and C-S-H in terms of kinetics, microstructure changes and moisture properties. *Cem. Concr. Res.* 56, 153–170. doi:10.1016/j.cemconres.2013.11.015

Niel, P., and Eurybiades, B. (1982). The solubilities of calcite, aragonite, and vaterite in CO_2-H_2O solutions between 0 and 90°C, and evaluation of the aqueous model for the system CaCO_3-CO_2H_2O. *Geochim. Cosmochim. Acta.* 46, 1011–1040.

Palmer, T. J., Hudson, J. D., and Wilson, M. A. (1988). Palaeoecological evidence for early aragonite dissolution in ancient calcite seas. *NATURE* 335 (6193), 809–810. No. doi:10.1038/335809a0

Poudyal, L., Adhikari, K., and Won, M. (2021). Mechanical and durability properties of portland limestone cement (PLC) incorporated with nano calcium carbonate ($CaCO_3$)(Article). *MATERIALS* 14 (4), 1–19. No.

Rostami, V., Shao, Y., Boyd, A. J., and He, Z. (2012). Microstructure of cement paste subject to early carbonation curing. *Cem. Concr. Res.* 42 (1), 186–193. No. doi:10.1016/j.cemconres.2011.09.010

Sánchez Herrero, M. J., Fernández Jiménez, A., Palomo, Á., and Klein, L. (2016). Alkaline hydration of C_2S and C_3S. *J. Am. Ceram. Soc.* 99 (2), 604–611. No. doi:10.1111/jace.13985

Shah, V., Scrivener, K., Bhattacharjee, B., and Bishnoi, S. (2018). Changes in microstructure characteristics of cement paste on carbonation. *Cem. Concr. Res.* 109, 184–197. doi:10.1016/j.cemconres.2018.04.016

Shen, Q., Pan, G., and Bao, B. (2016). Influence of CSH carbonation on the porosity of cement paste. *Mag. Concr. Res.* 10, 504–514. No. doi:10.1680/jmacr.15.00286

Sorrentino, F. (2008). Upscaling the synthesis of tricalcium silicate and alite. *Cem. WAPNO BETON* 8 (4), 177. No.

Tadros, M. E., Skalny, J., and Kalyoncu, R. S. (1976). Early hydration of tricalcium silicate. *J. Am. Ceram. Soc.* 59 (7-8), 344–347. No. doi:10.1111/j.1151-2916.1976.tb10980.x

Therese, K. F., Eric, H. O., Sigurður, R. G., and Per, A. (2011). The effect of dissolved sulphate on calcite precipitation kinetics and consequences for subsurface CO_2 storage. *Energy Procedia* 4, 5037–5043. doi:10.1016/j.egypro.2011.02.476

Wang, D., Xiong, C., Li, W., and Jun, C. (2020). Growth of calcium carbonate induced by accelerated carbonation of tricalcium silicate. *ACS Sustain. Chem. Eng.* 8 (39), 14718–14731. No. doi:10.1021/acssuschemeng.0c02260

Wei, Tingcong, Wei, Fengqi, Zhou, Jinghong, Wu, Zhiqiang, Zhang, Chunmei, Jia, Zhuang, et al. (2022). Formation and strengthening mechanisms of xonotlite in C_3S-silica and C_2S-silica powder systems under high temperature and pressure. *Cem. Concr. Res.* 157, 106812. doi:10.1016/j.cemconres.2022.106812

Zuddas, P. P., Zuddas, U., Pachana, K., and Faivre, D. (2003). The influence of dissolved humic acids on the kinetics of calcite precipitation from seawater solutions. *Chem. Geol.* 201 (1), 91–101. No. doi:10.1016/s0009-2541(03)00230-4